UC San Diego
UC San Diego Previously Published Works

Title
Particle concentration and mixing in microdrops driven by focused surface acoustic waves

Permalink
https://escholarship.org/uc/item/4k79k896

Journal
Journal of Applied Physics, 104(1)

ISSN
0021-8979

Authors
Shilton, Richard
Tan, Ming K
Yeo, Leslie Y
et al.

Publication Date
2008-07-01

DOI
10.1063/1.2951467

Peer reviewed

Particle concentration and mixing in microdrops driven by focused surface acoustic waves

Richard Shilton, Ming K. Tan, Leslie Y. Yeo, and James R. Friend[a)]
Micro/Nanophysics Research Laboratory, Monash University, Clayton, VIC 3800, Australia

We report the use of focused surface acoustic waves (SAWs) generated on 128° rotated *Y*-cut *X*-propagating lithium niobate (LiNbO$_3$) for enhancing the actuation of fluids and the manipulation of particle suspensions at microscale dimensions. In particular, we demonstrate increased efficiency and speed in carrying out particle concentration/separation and in generating intense micromixing in microliter drops within which acoustic streaming is induced due to the focused SAW beneath the drop. Concentric circular and elliptical single-phase unidirectional transducers (SPUDTs) were used to focus the SAW. We benchmark our results against a straight SPUDT which does not cause focusing of the SAW. Due to the increased wave intensity and asymmetry of the wave, we found both circular and elliptical SPUDTs concentrate particles in under 1 s, which is one order of magnitude faster than the straight SPUDT and several orders of magnitude faster than conventional microscale devices. The concentric circular SPUDT was found to be most effective at a given input power since it generated the largest azimuthal velocity gradient within the fluid to drive particle shear migration. On the other hand, the concentric elliptical SPUDT generated the highest micromixing intensity due to the more narrowly focused SAW radiation that substantially enhances acoustic streaming in the fluid. © *2008 American Institute of Physics.*
[DOI: 10.1063/1.2951467]

I. INTRODUCTION

Microfluidic lab-on-a-chip devices for high throughput drug screening offer the possibility of working with tiny amounts of fluids, which can significantly reduce costs incurred by the reduction in the volumes of expensive reagents required.[1] The increased surface per unit volume also allows the enhancement of heat and mass transfer within the fluid. In addition, microfluidics also allows for the possibility of portability. With such technology, portable medical diagnostics kits and biosensors for fast detection of diseases and pathogens are now a real possibility. In the past decade, microfluidic research has grown exponentially due to the vast potential of its exploitation in a wide range of chemical, biological, and biomedical applications. Examples of these applications as well as fundamental issues associated with microfluidics can be found, for example, in Stone *et al.*,[2] Squires and Quake,[3] and references therein.

The concentration of particle suspensions is an important procedure in microfluidic processes. For example, the separation of red blood cells from plasma is an important and necessary pretreatment step in blood diagnostics.[4–6] Biosensors that act as early warning detection systems against airborne pathogenic threats also benefit from sample preconcentration to facilitate easier detection owing to current limitations of sensor technology that prohibit detection at ultralow concentrations. Recently, nanocolloid-based diagnostics have emerged as a powerful tool for miniaturized platforms for disease detection.[7] However, such technology relies on the ability to rapidly concentrate fluorescent-tagged nanobeads prior to the immobilization of the biological entities in order to provide a detectable fluorescent signal. While particle concentration and separation in suspensions is a standard laboratory process—using a centrifuge, for example—it is considerably more difficult to reproduce such effects at the microscale owing to the dominance of surface and viscous forces over body forces. Some techniques, such as evaporation-based sample concentration,[8] have been proposed, but these could be impractical in many applications because of the need to keep the sample hydrated. More recently, particle concentration via azimuthal microfluidic liquid recirculation has been demonstrated using electrohydrodynamic[4,5,9] and surface acoustic wave[6] (SAW) devices.

Due to the low Reynolds numbers at these scales, the generation of turbulence to effect mixing is equally difficult. However, there has been some progress in micromixing, with two main categories: (i) passive mixers which rely on diffusion or chaotic advection in the absence of any external energy input, and (ii) active mixers using external energy to drive the mixing process.[10] Relying on diffusion for passive mixing, in particular, leads to unreasonably long mixing times when working on the microscale as the diffusion time scales as $T \sim L^2/D$, where L is the characteristic length scale of the system and $D \sim 10^{-9}$ is the diffusion coefficient. Enhancing diffusivity or avoiding it by promoting chaotic mixing in passive mixers typically relies on complex, and therefore inconvenient geometries in mixing channels. Many active mixer designs have been investigated to avoid such problems, exploiting pressure,[11] dielectrophoresis,[12] thermal,[13,14] and other forcing mechanisms.[10] The same liquid recirculation generated using electrohydrodynamics and

a)Electronic mail: james.friend@eng.monash.edu.au.

SAWs for particle concentration can be used to drive dispersion instead of concentration to achieve effective micromixing.[4,6]

The focus of this paper will be on using focused SAWs to drive microfluidic bulk liquid recirculation for rapid particle concentration and micromixing. A typical SAW device consists of a pair of interdigital transducers (IDTs) patterned onto a piezoelectric substrate. A sinusoidally varying electric field is induced between adjacent metal electrode strips that generate strain within the piezoelectric substrate through the inverse piezoelectric effect. Depending on the piezoelectric crystal orientation and composition, different types of acoustic waves can be generated, such as flexural plate waves, Love waves, shear-horizontal SAWs (transverse particle displacements polarized parallel to the surface), and Rayleigh SAWs (axial particle displacements polarized normal to the surface).[15] Placing the IDT such that the strain field is induced along the X direction with a 128° rotated Y-cut X-propagating lithium niobate (LiNbO$_3$) (LN), the coupled electric, stress, and strain fields propagate as a Rayleigh-SAW on the piezoelectric substrate.

The ability for SAWs to drive microfluidic actuation lies in the coupling between the fluid and substrate. Due to the mismatch in sound velocities in the fluid and substrate, a SAW launched from an IDT and traveling along the substrate will be radiated into a fluid drop placed in its path at an angle of Θ_R from an axis normal to the surface and along the original direction of propagation, as depicted in Fig. 1(a). For an infinite half-space, the angle is given by the ratio of the SAW velocity along the substrate in the X direction and within the fluid,[16] i.e., $\Theta_R = \sin^{-1}(c_w/c_s)$, which is known as the Rayleigh angle. At room temperature, $c_s \approx 3990$ m/s in the absence of fluid loading and $c_w \approx 1450$ m/s for water, thus giving $\Theta_R \approx 23°$. Due to this leakage of radiation into the fluid, a longitudinal pressure wave is generated within the drop at the Rayleigh angle,[17] the pressure of which is given by

$$p_s = \rho_0 c_s^2 \left(\frac{\Delta\rho}{\rho_0}\right)^2, \tag{1}$$

where $\Delta\rho$ is the difference between the equilibrium density in the fluid ρ_0 and the fluid density at the crests and troughs of the SAW ρ. This pressure wave then drives acoustic streaming in the drop in a direction parallel to the acoustic radiation within the fluid[16,18] (hereafter referred to as the primary streaming flow). Bulk liquid recirculation occurs as a consequence of the closed volume of the drop. The induced primary streaming velocities inside a microdroplet are large in comparison to other schemes[19] (typically 10 mm/s, depending on the electrical power input, drop size, and type of fluid). The forces due to fluid streaming are sufficient to lift and transport solid objects placed within the drop, as demonstrated in Fig. 1(b) and originally demonstrated by Sano *et al.*[20] In addition, with the application of sufficient power in generation of the SAW, nonlinear acoustic phenomena within the fluid[16,21–24] may be exploited for drop translation and other fluid actuation schemes, to be discussed further later. In any case, it can be seen that the advantage of driving microfluidic actuation using SAW lies in the large amount of en-
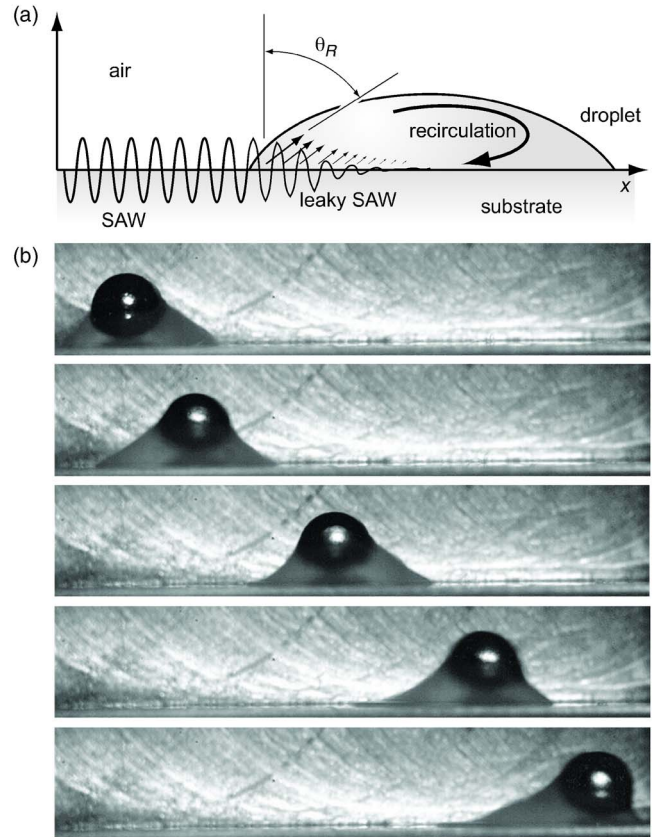

FIG. 1. (Color online) (a) Surface acoustic waves are radiated into the drop at the Rayleigh angle Θ_R, causing bulk recirculation within the drop. (b) The pressure wave at the Rayleigh angle that generates the fluid recirculation is sufficiently strong to generate a lift force on a 2 mm diameter steel ball placed on the 5 μl drop, akin to the phenomena described by Sano *et al.*(Ref. 43). Consequently, the ball levitated above the substrate surface within the drop and transported along the direction of SAW propagation, which is from left to right in the image.

ergy that may be radiated into the fluid with relative ease: up to 100 W may be delivered into a region 10 mm wide with a standard IDT.[25] Moreover, the generation of SAW is relatively straightforward and is widely used in inexpensive microdevices for the telecommunications industry.[26]

Tan *et al.*[27] showed that SAW may be exploited to pump liquids in microchannels at velocities up to several centimeters per second, typically one or more orders of magnitude higher than currently available micropump technology.[19] In particular, he showed that using electrokinetics—which is the current method of choice in microfluidics[2]—similar translation speeds[28] are also possible with discrete drops in open microfluidic platforms, far exceeding that possible with electrowetting.[29] On the other hand, Li *et al.*[6] demonstrated that it is possible to generate a net azimuthal component to the acoustic streaming by breaking the symmetry in the distribution of SAW radiation along the width of a drop and transverse to the radiation propagation direction. We shall refer to this as the secondary azimuthal flow. Figure 2 shows that this induced secondary azimuthal flow has sufficient momentum to carry along with it a 0.5 mm diameter steel ball on the surface of a 5 μl water droplet. By adjusting the IDT aperture width and driving a pair of IDTs set along the X
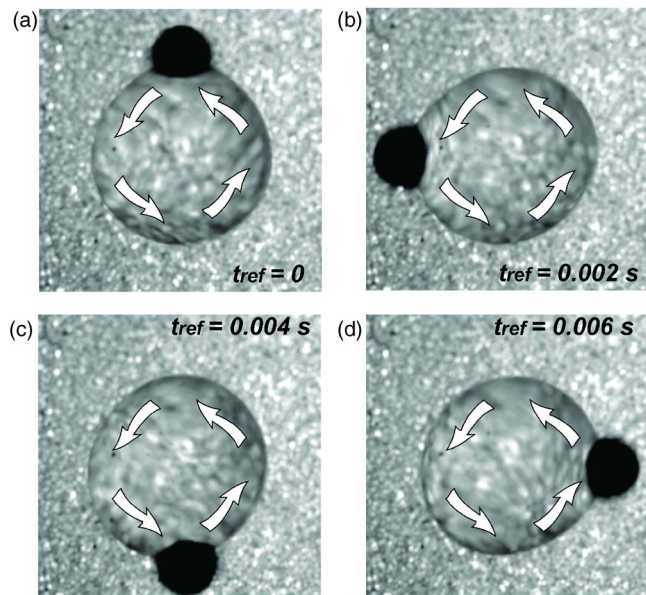
FIG. 2. (Color online) A 0.5 mm diameter steel ball placed within a 5 μl water drop atop a Teflon-coated lithium niobate substrate spins at over 6000 rpm due to the secondary azimuthal flow induced within the drop as a consequence of the asymmetric SAW radiation passing into the drop.

axis, Ito *et al.*[30] were able to induce single-pair and doubly paired vortices, respectively, within a fluid droplet set between the IDTs.

Microparticles in an aqueous suspension within a droplet may be concentrated out and deposited at the droplet's bottom center in around 15 s.[6] Such rapid concentration effects is in part due to particle migration under shear gradients[4,31] between regions of high shear at the periphery of the drop due to the convection driven by streaming phenomenon and regions of low shear at the center of the drop where the linear velocities become negligible. There is a roughly quadratic relationship between the applied power and strength of the concentration effect,[6] and so at very low and comparatively high powers the particles become dispersed. While particle dispersion is a potentially useful tool in some microfluidics applications, the upper bound on input power for effective particle concentration prevents one from reducing the concentration time for practical microfludics devices to less than around 10 s. In this work, we investigate the effect of focusing the SAW radiation on the substrate to a narrow region far smaller than the IDT aperture to increase the amount of radiation passing into the fluid drop. This is accomplished using an electrode-width-controlled (EWC) single-phase unidirectional transducer (SPUDT), originally proposed by Hartmann *et al.* over 25 years ago for telecommunications.[32] In doing so, the time required to perform concentration will be shown to decrease by one order of magnitude while using lower input powers than previously reported,[6] representing concentration times one to two orders of magnitude faster than electrohydrodynamics[4,5,9] commonly used in active microfluidics devices. Further, in calculating the effective mixing diffusivities with these devices in comparison to prior SAW systems, we show significant improvements in the speed of mixing on small scales.

Indeed, the effectiveness of using such focusing trans-

ducers for enhancing microfluidic actuation—in particular, particle concentration and micromixing—is the subject of this paper. In Sec. II, we begin with a brief review of the transducer design followed by a discussion of the use of focusing transducers to intensify SAW radiation at dimensions relevant to microfluidics. A comparison of two focused SPUDT designs and a conventional straight SPUDT is made using the results of particle concentration and micromixing experiments as presented in Sec. III and discussed in Sec. IV.

II. INTERDIGITAL TRANSDUCERS

White and Voltmer[33] first reported the direct generation of SAW on a piezoelectric substrate using an IDT, dramatically simplifying the process of generating useful low-loss, megahertz (MHz)-order acoustic waves. The fundamental building block of the conventional IDT design is a pair of straight metallic electrodes placed some distance away from each other and perpendicular to the wave propagation direction. Repeating this building block many times in constructing a single IDT increases the piezoelectric electromechanical coupling and maximum input power while sacrificing bandwidth. When the IDT is driven with a sinusoidal signal at the resonance frequency associated with the widths of the electrodes and the gaps between them (typically the same), local mechanical strains along the positive and negative *X*-axis direction are generated, producing elastic waves in both these directions. These bidirectional IDTs, although commonly used,[6,16] are not the most convenient or indeed efficient as the SAW that propagates from the IDT toward the nearest edge of the substrate are usually absorbed by a damping material placed atop the substrate to prevent wave reflection back into the device. More complex designs, including tuned reflectors and energy circulation techniques,[25] are possible; the SPUDT itself offers internally tuned reflectors within the IDT to form a unidirectional SAW propagating from only one side of the IDT (Ref. 34) through wave superposition between transmitted and reflected waves within the IDT. Stronger reflection within the IDT to more completely suppress SAW propagation in a direction opposite the desired direction is achievable by depositing higher density metals, such as Cu, to form the electrodes.[35]

An increase in SAW intensity is made possible by focusing the IDT using curved electrodes. The intensity increase is especially significant at the focus;[36] a review of such IDT configurations is provided in Wu *et al.*[37,38] The focused wave profile depends on the geometrical shape of the transducer; the most common shapes are concentric circular and concentric elliptical geometries. It is worth noting, however, that the focusing transducers in Wu *et al.*[37,38] are bidirectional.

The transducers used in this study combine the unidirectional propagation characteristics of the SPUDT configuration with curved electrodes to deliver the acoustic radiation to a smaller area near the focus of the IDT. A comparison of the effects of focusing is provided by using a straight EWC-SPUDT [Fig. 3(a)] along with two focusing elliptical EWC-SPUDTs with eccentricities of approximately 0.831 (E1) and 0.616 (E2), respectively [Figs. 3(b) and 3(c)], and a circular EWC-SPUDT [Fig. 3(d)]. Each of these transducers had 30
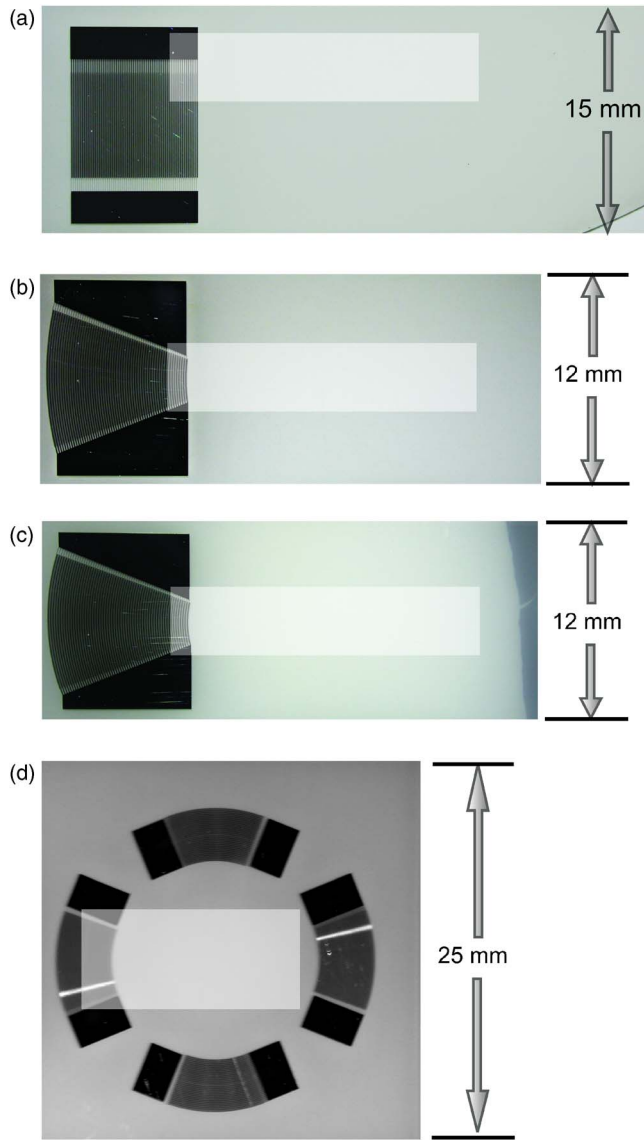
FIG. 3. (Color online) The SPUDTs fabricated and used in this work, including a (a) 30 MHz straight SPUDT, a (b) 30 MHz focusing elliptical SPUDT (E1) with an approximate eccentricity of 0.616, a (c) 30 MHz focusing elliptical SPUDT (E2) with an approximate eccentricity of 0.831, and a (d) 30 MHz focusing circular SPUDT. The vibration displacement perpendicular to the substrate surface was measured using a scanning laser vibrometer across the area highlighted in each image; the results of the vibrometer scans are shown in Fig. 4.
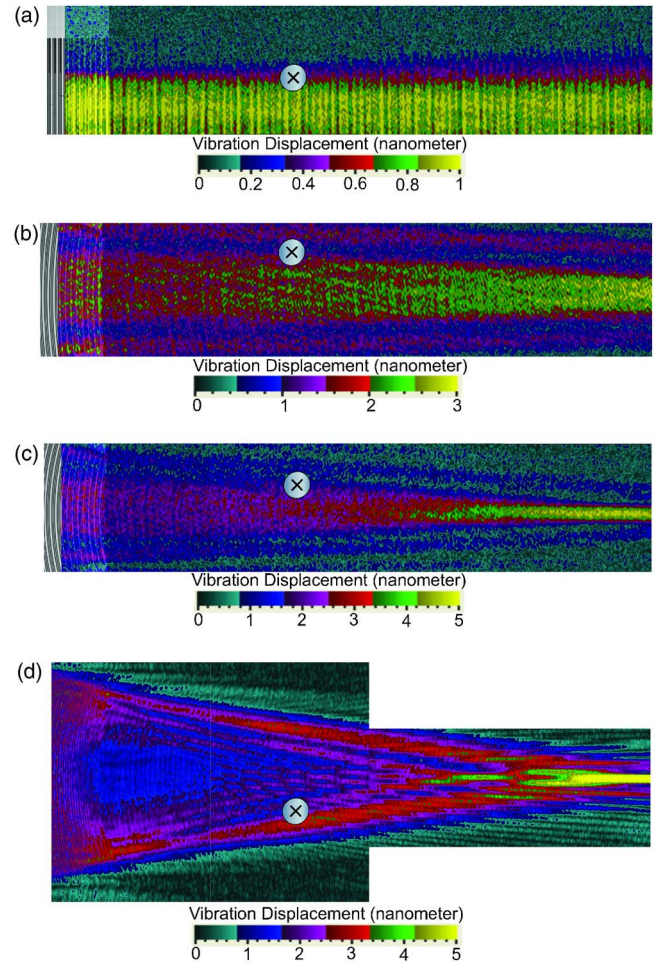

FIG. 4. (Color online) The amplitude of surface displacement perpendicular to the lithium niobate substrate surface as SAW propagates from (a) a straight SPUDT, (b) a concentric elliptical SPUDT with eccentricity 0.831 (E1), (c) a concentric elliptical SPUDT with eccentricity 0.616 (E2), and (d) a concentric circular SPUDT. The scanned area for each transducer corresponds to the highlighted area shown in Fig. 3. Each cross indicates the position at which a drop will be placed to study SAW-induced mixing and particle concentration and dispersion.

pairs of electrodes and were fabricated on 0.5 mm thick, 127.68° $Y-X$ LN single crystal substrates using standard photolithography processes. Dual-layer metallization was used for the transducer fabrication to enhance the bonding quality of the electrodes with a 25 μm thick Al layer sputtered on top of a 4 nm Ti adhesion layer. Applying a sinusoidal electrical signal at the fundamental resonant frequency of the IDTs (30 and 50 MHz) generates a SAW which propagates along the X axis. The major axis of the concentric elliptical transducers is perpendicular to the X axis. The substrates were each coated with a thin layer of amorphous Teflon (Teflon AF, DuPont Corporation), to prevent the droplet from spreading during induced rotation. Drop translation was avoided by employing applied power levels below that which is necessary to cause translational movement.[28] Figure

4 shows the SAW propagation patterns obtained using scanning laser Doppler vibrometry (LDV) (Polytec PI MSA-400, Waldbrunn, Germany) for the straight SPUDT, the elliptical (E1 and E2) SPUDTs, and the circular SPUDT. A comparison between Figs. 4(a) and 4(b) clearly shows that focusing of the SAW into a high intensity beam along the focal line of the transducer is achieved with the use of the elliptical SPUDT. By further reducing the eccentricity of the elliptical geometry, the focused beam becomes more narrow and intense.

Figure 4(c) shows a highly intensified SAW at a distance of approximately 7 mm from the SPUDT aperture with a smaller eccentricity of 0.616. The SAW eventually focuses to a spot when the eccentricity decreases to zero, in which case the ellipse becomes a circle, as seen in Figs. 4(c) and 4(d). The cross in each figure panel indicates the approximate location where a droplet was dispensed and irradiated with SAW to perform micromixing or particle concentration and dispersion. The locations were selected along the edges of the SAW radiation field in the substrate in order to generate

an asymmetric radiation field across the width of the droplet; in each case the distance of the drop from the IDT's output aperture was fixed at 5 mm.

The width of the SAW from an IDT with straight electrodes is typically taken to be the same as the aperture width and is usually very close to this value over even long distances in comparison to the wavelength. For the focused SPUDT configurations, there are similar approximations using straight lines drawn out from the IDT in a manner analogous to optics, but from Fig. 4 it is evident that this approach is error-prone: the boundaries of the SAW radiation are quite curved. Mapping surface vibrations using the LDV is time consuming and is limited by the upper frequency range of the vibrometer, 40 MHz with the Polytec MSA-400. Tan *et al.*[39] proposed a new method in visualizing the focused SAW using smoke particles. This method has three advantages over the LDV. It works at frequencies up to at least 500 MHz, an order of magnitude larger than our LDV. More importantly, the time required to scan SAW wave propagation on one 30 MHz device is reduced from four hours using the scanning LDV—like other, even "high-speed" holography techniques that require some time for analysis[40,41]—to only 60 s using this method. Finally, the technique requires little more than smoke and careful observation in contrast to the complexity of interferometry and holography.

III. EXPERIMENTS

To generate bulk liquid recirculation in the drop, symmetry breaking of the SAW radiation distribution along the drop width transverse to the SAW propagation direction is necessary.[6] In this work, the drop is placed asymmetrically along one side of the SAW propagation pathway such that it only experiences the radiation across a fraction of its width. As indicated earlier, the position at which the drop is placed is indicated by the crosses in Fig. 4 for each transducer.

A. Rotational speeds

The bulk rotation speed within the drop was compared for three different transducers, i.e., the 50 MHz concentric circular, elliptical (E1) and straight SPUDTs, over a range of input powers (10–100 mW) at the resonant frequency. In each case, 5 μl drops of water containing 5 μm fluorescent polystyrene particles (BioScientific, Gymea NSW) were dispensed 5 mm from the leading edge of the transducer at the position approximately shown in Fig. 4. The drop rotation was recorded via high-speed video (Olympus iSpeed) at a speed of 100 frames per second through a stereomicroscope (Olympus BXFM, Tokyo, Japan) under fluorescent illumination supplied by an EXFO X-Cite 120 mercury light source and a proprietary 120 W short arc lamp (Olympus, Tokyo, Japan). Average linear particle velocities were then extracted from image frame grabs from the video files using standard commercially available particle tracking software (Diatrack 3.01, Semasopht, Chavannes, Switzerland). Examples of the particle trajectories from which the velocities are estimated are shown in Figs. 5(a) and 5(b) for low and high applied powers, respectively.
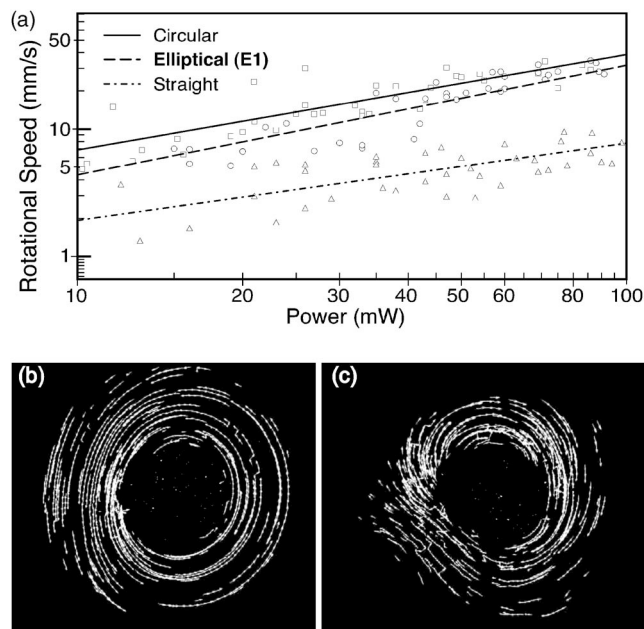

FIG. 5. (a) Linear rotation speeds for different input powers for the concentric circular, elliptical (E1) and straight SPUDTs. Images (b) and (c) show the particle trajectories as they recirculate within the 5 μl drop, which were analyzed using the particle tracking software Diatrack to determine the rotational velocities. The images (b) and (c) are for low ($<$50 mW) and high ($>$50 mW) power excitation, respectively.

B. Particle concentration

The time required to concentrate microparticles out of a homogeneous aqueous suspension for a variety of input powers was measured with each of the different 30 MHz SPUDT designs. Fluorescent polystyrene particles 0.5 μm in diameter (Duke Scientific, Victoria, Australia) were diluted in deionized water to a concentration of approximately 0.1% of solid particles. The 0.5 μl drops of these particle suspensions were then placed 5 mm from the SPUDT aperture at the periphery of the focused region of the propagating wave, as illustrated in Fig. 4.

The progress of the concentration process was observed via the same high speed video microscopy system described earlier. The concentration process was repeated three times for each parameter set and the concentration times were averaged across these runs. Specifically, the concentration time was determined by plotting the normalized standard deviation of the pixel intensity of the grayscale video frames against time. The standard deviation of the pixel intensity was normalized with respect to the standard deviation of the first frame and the final (highest) standard deviation. The concentration time is defined as the time when the normalized standard deviation first reaches its minimum value. Concentration times were obtained for each SPUDT design at input powers between 100 and 700 mW, the upper limit being the highest power that can be applied to the drop without causing it to translate linearly along the SAW propagation direction.[28]

C. Micromixing

The same set of SPUDT designs were used to compare micromixing efficacy. A 0.5 μl deionized water drop dyed

nearly black with blue food dye was carefully pipetted onto a 2 μl drop of transparent glycerine very lightly dyed with green food dye and placed directly on the Teflon-coated surface. The water drop was slowly pipetted onto the glycerin free surface to avoid mixing due to inertial currents arising from the impact of the drop; the relatively high viscosity of glycerine was beneficial in this regard. The mixing process was captured via the same high-speed video microscopy system described earlier under reflected bright-field illumination at a frame rate of 60 frames/s. To quantify the mixing of the drops, a pixel intensity analysis was carried out on the image frame grabs from the video files after they were converted to grayscale images. The logarithm of the standard deviation was normalized with respect to the logarithmic standard deviation of the first frame. The variation of the normalized logarithm of the standard deviation was then plotted versus time for different input powers.

By assuming a purely diffusive mechanism by which the micromixing occurs, the spreading of area of the dyed region will occur exponentially with respect to time. A measure of the mixing intensity, as quantified through the diffusion coefficient D, may be determined approximately from a linear regression of the plot of the normalized standard deviation in the pixel intensity against time.[42] More specifically, the gradient of the slopes in the plots of the normalized logarithm of the standard deviation of the pixel intensity as a function of time is proportional to $-D/L^2$, where L is the characteristic length scale of the drop.

IV. RESULTS AND DISCUSSION

The linear rotation speed of the particles over a range of powers for each SPUDT design is shown in Fig. 5(a). The figure shows a significant increase in the rotational velocity for the concentric circular and elliptical SPUDTs over that of the straight SPUDT, which is expected due to the increase in the asymmetry of the SAW radiation into the drops.

The linear rotational velocities associated with the circular SPUDT are slightly faster than with the elliptical (E1) SPUDT. The circular SPUDT focuses the SAW radiation at a single point, unlike the elliptical (E1) SPUDT, as seen in Fig. 3. Because of this focusing mechanism, the circular SPUDT delivers the largest amplitude SAW radiation into the drop, but the irradiated region is smaller, generating strong but localized acoustic streaming. The elliptical (E1) SPUDT spreads a similar amount of SAW radiation over a larger width upon interaction with the drop, causing the generation of liquid recirculation over a longer length scale.

Figure 6 shows sequential images of the induced drop rotation which acts to rapidly concentrate the suspended particles toward the center of the drop on the substrate for a concentric circular SPUDT. Similar concentration patterns were observed for the concentric elliptical (E2) and straight SPUDTs. Figure 7 shows the normalized standard deviation of the pixel intensity against time for three different input powers for the concentric circular SPUDT, indicating the concentration time is decreased as the input power (and therefore the SAW amplitude) is increased. Qualitatively, the
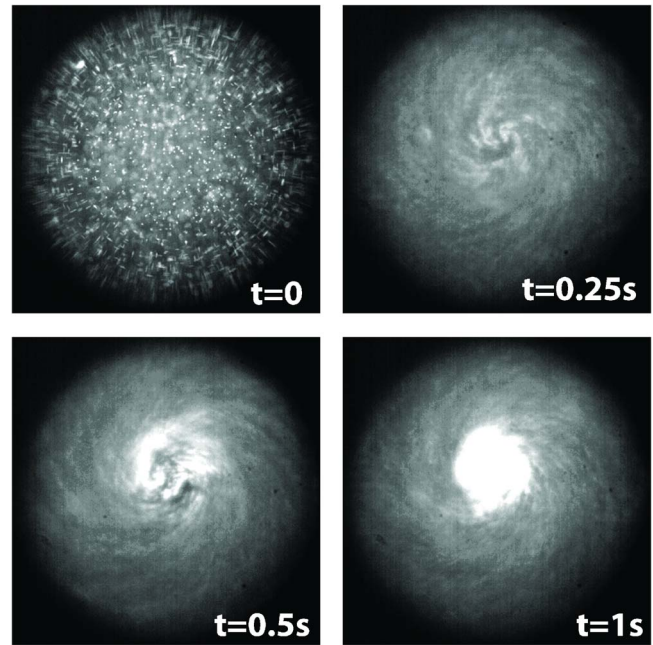

FIG. 6. (Color online) Concentration of particles in the 0.5 μl drop via drop rotation induced by acoustic radiation from the focused elliptical SAW. Similar patterns were observed for the concentration driven by the circular and straight SPUDTs.

concentration behavior is similar for all the SPUDT devices, though the speeds at which the concentration occurs for each SPUDT design differs.

The time to achieve particle concentration versus a range of powers for each SPUDT design is provided in Fig. 8, again demonstrating the superior performance of the focusing SPUDTs over the straight SPUDT. In both of the focusing SPUDT designs, we note that the particle concentration time is extremely rapid, occurring in just under 1 s. The difference in the concentration times can be explained by recalling the mechanism by which the particles concentrate: shear-induced migration arising due to the shear gradients across the radial axis of the drop from SAW-driven streaming. The larger the shear gradient, the faster the particles are transported into the center of the droplet. The particle concentration times for each SPUDT design in Fig. 8 are there-
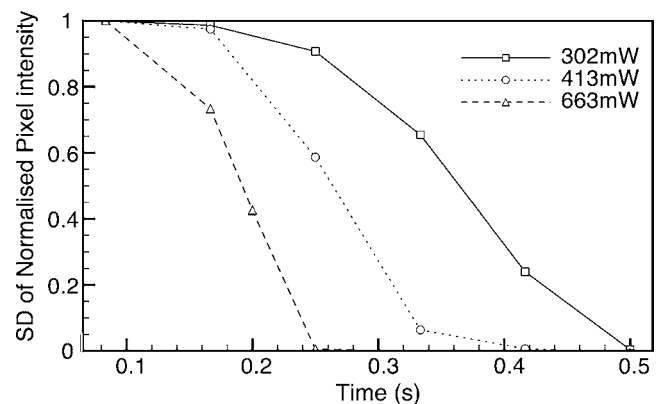

FIG. 7. The normalized pixel intensity is a measure of the particle concentration; plotted here against time using the concentric circular SPUDT at different power levels it shows an increase in input power reduces the time required to concentrate the particles out of suspension.
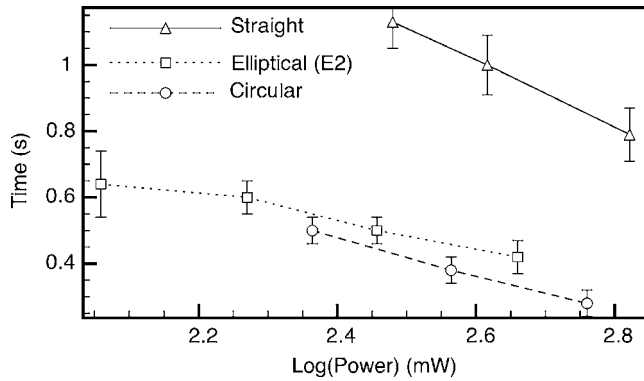
FIG. 8. Particle concentration times as a function of the applied power for the concentric circular, elliptical (E2), and straight SPUDTs.
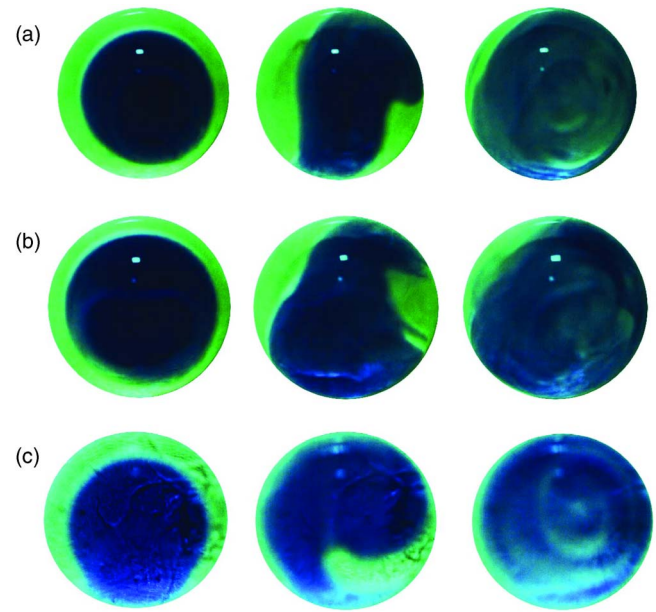

FIG. 9. (Color online) Rapid mixing of water (dark) mixed with glycerine (light) using the (a) concentric circular, (b) elliptical (E1), and (c) straight SPUDT designs. For (a), the images at $t=0$, 0.55, and 1.2 s are shown. For (b), the images at $t=0$, 0.633, and 1.35 s are shown. For (c), the images at $t=0$, 0.9, and 1.9 s are shown.

fore consistent with the results for the velocity measurements shown in Fig. 5(c). At the center of the drop, the linear velocity approaches zero. As such the shear gradient depends predominantly on the linear rotational velocity at the periphery of the drop. Given that this is the largest for the circular SPUDT and the smallest for the straight SPUDT, it then follows that the shear gradients are the largest and smallest for these two cases, respectively. Consequently, the particle concentration times are the fastest for the circular SPUDT and the slowest for the straight SPUDT.

With the drop placed on the edge of the focused SAW region for each SPUDT, as indicated in Fig. 4, it would be expected that the circular SPUDT would lead to the shortest concentration time, followed by the elliptical SPUDT and then the straight SPUDT. A similar arrangement would be expected for drop rotational speeds. Figures 5 and 8 confirm and demonstrate that for rotational speeds and concentration the circular SPUDT is best, while the straight SPUDT is worst.

Figures 9(a)–9(c) show the progression of mixing of the dyed water (dark) with the dyed glycerine solution (light) for each of the three SPUDT designs. The normalized standard deviation of the pixel intensities of grayscale versions of these images are plotted as a function of time for each SPUDT design over a range of input powers. In each case, the slopes of the curves in Figs. 10(a)–10(c) are proportional to $-D/L^2$. The effective diffusivity D_{eff} increases as the input power is increased due to convective-driven mixing effects arising from the imposed SAW-driven bulk liquid recirculation. The slope of the pixel intensity with respect to time in the absence of SAW driven convection had a value of -0.0014 for the drop which was of the order of $L \sim 10^{-3}$ m, giving a value of $D_0 \sim 10^{-9}$ m^2/s, consistent with typical values for the diffusion coefficient associated with these fluids.

Given that D_{eff}/D_0 provides a measure of the mixing enhancement due to the SAW-driven convection relative to molecular diffusion in the absence of convection, we show in Fig. 11 a comparison of this mixing enhancement for each SPUDT design. By using a log-log plot and determining the slope of the mixing enhancement versus time data for each SPUDT design, it is possible to compare the effectiveness of mixing in each design with a single parameter: the exponent

n at which the mixing enhancement scales with power, i.e., $(D_{eff}/D_0) \sim P^n$. Generally, the scaling occurs with values of n greater than or equal to 2. Specifically, it scales as $n=2$ for the straight SPUDT, $n=2.14$ for the elliptical (E1) SPUDT, and $n=2.3$ for the circular SPUDT.

It is interesting to note that the slope of the curves in Fig. 11 for each design is approximately similar, indicating that the mechanism by which the mixing is enhanced, in particular, by convective transport arising from the SAW-driven bulk recirculation, is the same. As such, the mixing diffusivity is always observed to scale in the same manner with respect to the input power. However, the effective diffusivity is the highest with the concentric elliptical (E1) SPUDT design and lowest with the concentric circular SPUDT design suggesting that they are the most and least effective transducers for micromixing, respectively.

In contrast to the particle concentration which is promoted by the secondary azimuthal flow about the vertical axis arising from the asymmetry induced along the width of a drop and transverse to the radiation propagation direction, convective enhancement of the micromixing process using the SAW-driven bulk liquid recirculation is predominantly driven by the primary streaming flow in the direction about the horizontal (transverse to the radiation propagation direction) axis arising due to the leakage of the acoustic energy from the substrate into the drop at the Rayleigh angle Θ_R. This is because the dye is pipetted at the vertex of the glycerine drop, as depicted in Fig. 12(a).

Since the beam focusing of the elliptical SPUDT provides the highest intensity of the SAW radiation into the drop, it then follows that the primary streaming flow is the strongest for this transducer configuration. Conversely, the intensity, and hence, the strength of the primary streaming flow is the weakest for the straight SPUDT. This hierarchical
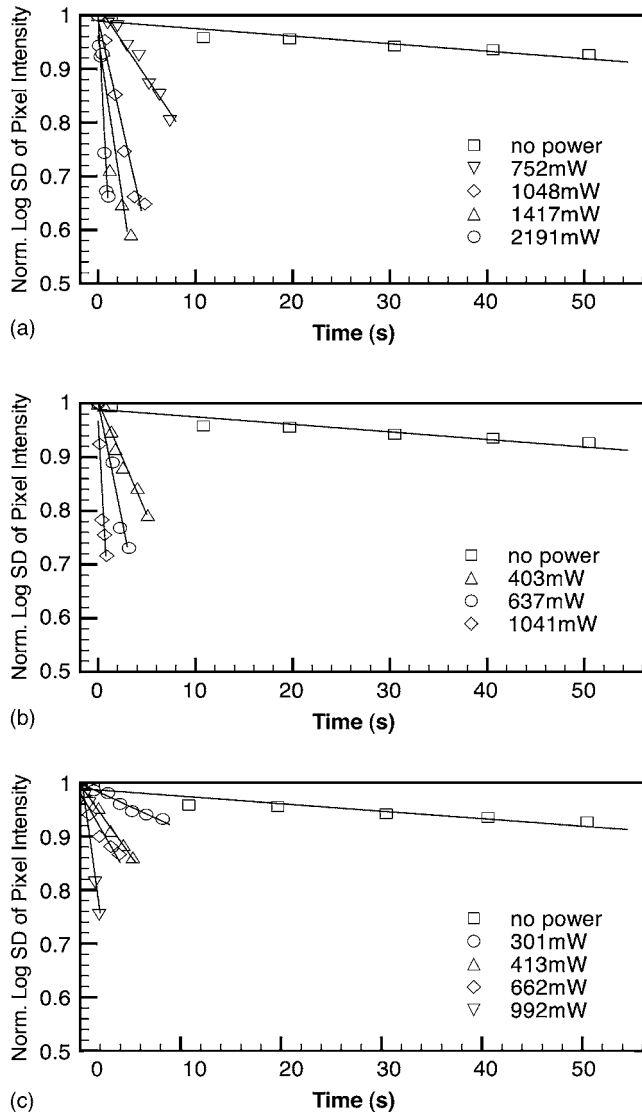
FIG. 10. Normalized standard deviation in the pixel intensity as a function of time for the (a) concentric circular, (b) elliptical (E1), and (c) straight SPUDT designs.

order therefore explains, at least qualitatively, why the elliptical SPUDT has the highest mixing diffusivity.

The role of the secondary azimuthal recirculation arising due to the asymmetry in the drop position in the pathway of the SAW propagation is less clear. This secondary flow could promote mixing to a certain extent at later stages once the primary flow has convected the dye to the deeper regions of the drop away from the drop vertex. But as can be seen in Fig. 9(b), the secondary azimuthal flow recirculates the dye most strongly in the outer periphery of the drop near its free surface. Since the primary streaming flow is weakest near the free surface, the secondary azimuthal flow could reduce the mixing enhancement induced by the primary flow. This could provide an explanation as to why the circular SPUDT, in which the secondary azimuthal rotational flow is the strongest, as observed in Fig. 5, has a lower mixing diffusivity than the straight SPUDT, despite having higher radiation intensities that give rise to stronger primary streaming flows. It should be noted though that our earlier observations are qualitative in nature given that we have employed a two-
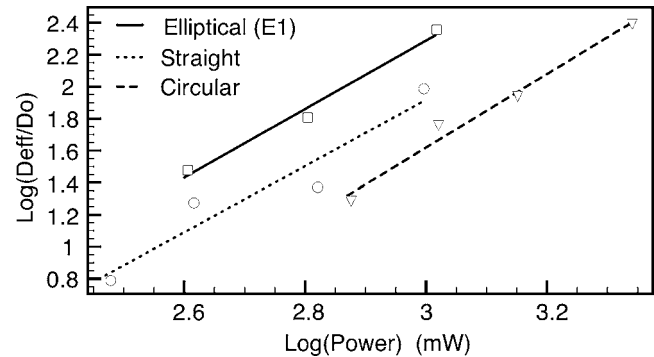

FIG. 11. Effect of the input power on the mixing enhancement, measured by the ratio of the effective diffusivity D_{eff} to the diffusivity due to pure diffusional mixing D_0 in the absence of SAW-driven convection when no power is applied.

dimensional pixel intensity analysis, independent of the channel depth. Consequently, mixing through the depth of the drop is only indirectly quantified.

V. CONCLUSIONS

Rapid concentration of suspensions of particles and mixing of fluids in microdrops was demonstrated by producing acoustic streaming in drops via focused SAWs using straight, concentric circular, and elliptical SPUDTs. We show that the focused SPUDTs increase the concentration speed over a straight SPUDT by at least one order in magnitude. Since the shear-induced migration mechanism requiring a radial gradient in the azimuthal velocities appears to govern the particle concentration, the SPUDT that produces the largest secondary azimuthal recirculation for a given power is the most effective for concentrating the particles. As such, the concen-
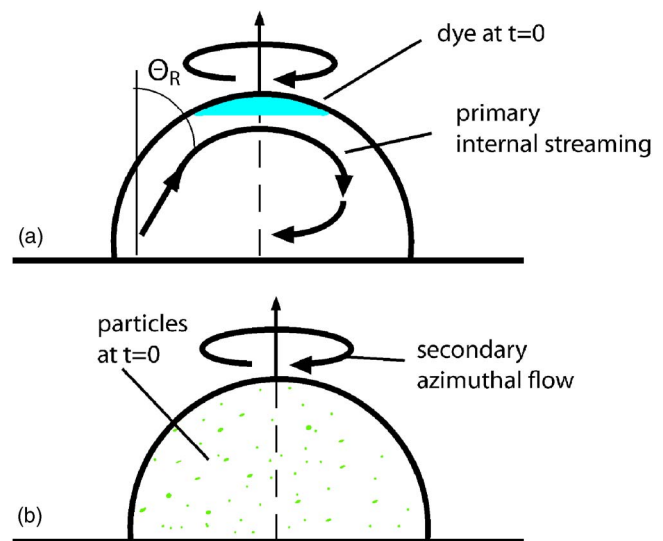

FIG. 12. (Color online) (a) Micromixing and (b) particle concentration in a drop driven by SAW-driven bulk liquid recirculation. For micromixing (a), the mixing of the dye placed at the top of the drop is promoted by the primary internal streaming flow arising due to direct leakage of the SAW radiation from the substrate at the Rayleigh angle Θ_R. The secondary azimuthal flow generated due to the asymmetric drop position on the substrate serves only to recirculate the dye. On the other hand, the concentration process is predominantly driven by particle shear-induced migration, which is promoted by the secondary azimuthal flow.

tric circular SPUDT was observed to be more efficient for particle concentration than the elliptical SPUDT. Nevertheless, we observe that both of these SPUDTs are able to concentrate the particles very rapidly in under 1 s. On the other hand, micromixing relies to a large extent on the primary acoustic streaming flow to transport the dye to the other regions of the drop of greater depth, especially in the present case when the dye is placed at the apex of the drop. With this arrangement, the elliptical SPUDT was observed to be the most effective for micromixing, increasing the effective diffusivity well beyond the results of the straight SPUDT. This is because the elliptical SPUDT provides the highest intensity of SAW radiation into the drop. In any case, these focusing SAWs provide a very rapid and effective mechanism for microfluidic manipulation, in particular, particle concentration and micromixing, which is one order of magnitude, if not several orders of magnitudes faster than current microfluidic technology.

ACKNOWLEDGMENTS

[1] B. Haab, A. Paulovich, N. Anderson, and A. Clark, Mol. Cell. Proteomics **5**, 1996 (2006).
[2] H. Stone, A. Stroock, and A. Ajdari, Annu. Rev. Fluid Mech. **36**, 381 (2004).
[3] T. Squires and S. Quake, Rev. Mod. Phys. **77**, 977 (2005).
[4] L. Yeo, D. Hou, S. Maheshswari, and H. Chang, Appl. Phys. Lett. **88**, 233512 (2006).
[5] D. Arifin, L. Yeo, and J. Friend, Biomicrofluidics **1**, 014103 (2007).
[6] H. Li, J. Friend, and L. Yeo, Biomed. Microdevices **9**, 647 (2007).
[7] H. Chang, AlChE J. **53**, 2486 (2007).
[8] G. Walker and D. Beebe, Lab Chip **2**, 57 (2002).
[9] L. Yeo, J. Friend, and D. Arifin, Appl. Phys. Lett. **89**, 103516 (2006).
[10] N. Nguyen and Z. Wu, J. Micromech. Microeng. **15**, R1 (2005).
[11] J. Zahn, A. Deshmukh, A. Pisano, and D. Liepmann, Proceedings of the IEEE Micro Electro Mechanical Systems (MEMS), 2001, pp. 503–506.
[12] J. Deval, T. Patrick, and C. Ho, Proceedings of the IEEE Micro Electro Mechanical Systems (MEMS), 2002, pp. 36–39.
[13] H. Mao, T. Yang, and P. Cremer, J. Am. Chem. Soc. **124**, 4432 (2002).
[14] J. Tsai and L. Lin, Sens. Actuators, A **97–98**, 665 (2002).
[15] S. Shiokawa and J. Kondoh, Jpn. J. Appl. Phys., Part 1 **43**, 2799 (2004).
[16] A. Wixforth, C. Strobl, C. Gauer, A. Toegl, J. Scriba, and Z. v. Guttenberg, Anal. Bioanal. Chem. **379**, 982 (2004).
[17] K. Sritharan, C. J. Strobl, M. Schneider, A. Wixforth, and Z. Guttenberg, Appl. Phys. Lett. **88**, 054102 (2006).
[18] L. Rayleigh, Philos. Mag. **10**, 364 (1905).
[19] D. Laser and J. Santiago, J. Micromech. Microeng. **14**, R35 (2004).
[20] A. Sano, Y. Matsui, and S. Shiokawa, Jpn. J. Appl. Phys., Part 1 **37**, 2979 (1998).
[21] W. L. Nyborg, in *Acoustic Streaming*, edited by W. P. Mason and R. N. Thurston (Academic, New York, 1965), Vol. 2B, Chap. 11, pp. 265–329.
[22] C. Bradley, J. Acoust. Soc. Am. **100**, 1399 (1996).
[23] A. Wixforth, Superlattices Microstruct. **33**, 389 (2003).
[24] Z. Guttenberg, A. Rathgeber, J. Radler, A. Wixforth, M. Kostur, M. Schindler, and P. Talkner, Phys. Rev. E **70**, 056311 (2004).
[25] M. Kurosawa, P. Nayanbuu, and K. Asai, Proceedings of the 2003 IEEE/ASME International Conference on Advanced Intelligent Mechatronics (AIM), Kobe, Japan, 20–24 July 2003, Vol. 2, pp. 1327–1331.
[26] C. Campbell, *Surface Acoustic Wave Devices for Mobile and Wireless Communications* (Academic, New York, 1998).
[27] M. Tan, J. Friend, and L. Yeo, in 16th Australasian Fluid Mechanics Conference (AFMC), Gold Coast, Australia, 2007a, pp. 790–793.
[28] M. Tan, J. Friend, and L. Yeo, Lab Chip **7**, 618 (2007).
[29] L. Yeo and H. Chang, Mod. Phys. Lett. B **19**, 549 (2005).
[30] S. Ito, M. Sugimoto, Y. Matsui, and J. Kondoh, Jpn. J. Appl. Phys., Part 1 **46**, 4718 (2007).
[31] D. Leighton and A. Acrivos, J. Fluid Mech. **181**, 415 (1987).
[32] C. Hartmann, P. Wright, R. Kansy, and E. Garber, Ultrasonics Symposium, 1982, pp. 40–45.
[33] R. White and F. Voltmer, Appl. Phys. Lett. **7**, 314 (1965).
[34] C. Hartmann and B. Abbott, Proc. IEEE **1**, 79 (1989).
[35] S. Nakagomi, H. Asano, H. Tanaka, T. Omori, K. Hashimoto, and M. Yamaguchi, Jpn. J. Appl. Phys., Part 1 **42**, 3152 (2003).
[36] S. Fang, S. Zhang, and Z. Lu, IEEE Trans. Ultrason. Ferroelectr. Freq. Control **36**, 178 (1989).
[37] T.-T. Wu, H.-T. Tang, Y.-C. Chen, and P.-L. Liu, IEEE Trans. Ultrason. Ferroelectr. Freq. Control **52**, 1384 (2005).
[38] T. Wu, H. Tang, and Y. Chen, J. Phys. D **38**, 2986 (2005).
[39] M. Tan, J. Friend, and L. Yeo, Appl. Phys. Lett. **91**, 224101 (2007).
[40] K. Hashimoto, H. Kamizuma, M. Watanabe, T. Omori, and M. Yamaguchi, IEEE Trans. Ultrason. Ferroelectr. Freq. Control **54**, 1072 (2007).
[41] K. Telschow, V. Deason, D. Cottle, and J. Larson III, IEEE Trans. Ultrason. Ferroelectr. Freq. Control **50**, 1279 (2003).
[42] S. Wang, Y. Lai, Y. Ben, and H. Chang, Ind. Eng. Chem. Res. **43**, 2902 (2004).
[43] A. Sano, Y. Matsui, and S. Shiokawa, Jpn. J. Appl. Phys., Part 1 **37**, 2979 (1998).